International Journal of Thermal Sciences 121 (2017) 336–347

Contents lists available at ScienceDirect

International Journal of Thermal Sciences

journal homepage: www.elsevier.com/locate/ijts

Transient thermal stress intensity factors for a circumferential crack in a hollow cylinder based on generalized fractional heat conduction

X.-Y. Zhang, X.-F. Li*

School of Civil Engineering, Central South University, Changsha 410075, PR China

ARTICLE INFO

Article history:
Received 27 January 2017
Received in revised form
27 February 2017
Accepted 18 July 2017

Keywords:
Generalized fractional heat conduction
Circumferential crack
Transient thermal stress
Thermal stress intensity factor
Cracked hollow cylinder

ABSTRACT

A generalized fractional heat conduction theory is applied to investigate the transient thermal fracture problem of a hollow cylinder with an embedded or surface circumferential crack. Integral transform technique is used to solve an associated initial-boundary value problem. Explicit temperature field and thermal stresses are given in the Laplace transform domain for a circumferentially cracked hollow cylinder subjected to thermal shock at the inner surface and with an insulated outer surface. Numerical results in the time domain are obtained by using numerical inversion of the Laplace transform. Transient thermal stresses induced by a crack are determined and thermal stress intensity factors at the crack front are calculated. The effects of fractional order, phase lag of heat flux on the transient temperature field, thermal stresses and thermal stress intensity factors are illustrated graphically for internal and surface cracks. The obtained results based on non-Fourier law of fractional heat conduction are compared with those using the classical Fourier law and hyperbolic heat conduction models, respectively.

1. Introduction

Thermal stress analysis of vessels and pipes is of particular interest, especially for those with defects like cracks. The presence of cracks results in very high thermal stresses near the cracks due to change in environment temperature, and this may cause catastrophic failure of a cracked structure. The most famous example is the explosion of Challenger shuttle after several seconds of ignition in 1986. Such vessels and pipes with crack are frequently encountered in engineering applications. A typical case is a hollow cylinder with embedded or surface crack subjected to heat shock and a great deal of work on fracture of cracked cylinders has been done. For example, Nied and Erdogan [1] analyzed an internal circumferential surface crack of a hollow cylinder suddenly cooled from the inside surface. Furthermore, the effect of cladding on the thermal shock resistance was also dealt with for a circumferentially cracked hollow cylinder [2]. Later, Meshii and Watanabe [3,4] obtained a series of results of stress intensity factors for circumferential cracks under radial temperature distribution or thermal striping. Kordisch et al. [5] studied initiation and growth of a circumferential crack in the HDR-RPV-cylinder under pressurized thermal shock. Dag et al. [6] further formulated circumferential crack problems of a functionally graded material cylinder subjected to temperature change. The finite element method was used to determine an accurate weight function for the crack and a closed-form thermal stress intensity factor with the aid of the weight function method was extracted by Nabavi and Ghajar [7]. For functionally graded cylinders with internal circumferential cracks, the thermal stress intensity factor expression was derived through the weight function method in Ref. [8]. The effect of heat conduction in a penny-shaped crack on thermal stress intensity factors was investigated in Ref. [9].

All of the above-mentioned studies are based on the classical Fourier's law. As well known, although it is widely used in many applications, an evident shortage is that heat diffusion behavior has infinite speed of propagation [10]. That is, if temperature at some point in a medium suddenly changes, it will be felt simultaneously at any other position in the medium. This unphysical hypothesis makes the classical Fourier heat conduction theory unacceptable, in particular for ultrafast heat transfer or extremely high temperature gradient. To overcome this disadvantage, many generalized heat conduction theories have been proposed such as hyperbolic heat conduction model [11,12], dual phase lag heat conduction model [13] and fractional heat conduction model [14], etc.

Within the framework of hyperbolic heat conduction theory, some researchers treated crack problems of cracked elastic media under heat shock (see e.g. Refs. [15,16]). In particular, Fu et al. [17,18] investigated the fracture behavior of a hollow cylinder containing a

* Corresponding author.
E-mail address: xfli@csu.edu.cn (X.-F. Li).

http://dx.doi.org/10.1016/j.ijthermalsci.2017.07.015
1290-0729/

circumferential crack under convective heat transfer boundary conditions and analyzed the effect of material properties on stress intensity factor of a circumferential crack. As pointed out in Ref. [19], the hyperbolic heat conduction equation predicts physically impossible negative thermal energies and is not a continuation of the classical model at very short time scales.

On the other hand, as a natural extension of the classical integer-order calculus, differential equations of fractional order have been developed to study various problems in science and technique [20,21]. Sherief et al. [22] and Youssef [23] respectively proposed new theories of thermoelasticity and generalized thermoelasticity using the methodology of fractional calculus with one relaxation time. Povstenko [24] considered theories of thermoelasticity based on all four fractional Cattaneo telegraph equations which are proposed in Ref. [25]. Due to its non-local property, implying that the next state of a system depends upon not only its current state but also all of its historical states, Qi and Liu [26] derived an analytical solution corresponding to the time-fractional radial heat conduction in some hollow geometries. Ezzat and EI-Bary [27] applied a fractional model to solve a problem of an infinite long hollow cylinder in the presence of an axial uniform magnetic field. Many representative results on fractional heat conduction in connection with thermal stresses can be found in Ref. [28]. These studies are limited to elastic media without defect. When some defects such as crack are present in media, how the fractional heat conduction affects thermal stresses is interesting. For an elastic layer with embedded and edge cracks, the effect of fractional order on thermal stresses was investigated recently [29]. Nonetheless, for a hollow cylinder with a circumferential embedded or surface crack, when the fractional heat conduction theory is adopted under heat shock at the cylinder surface, there is no information available on transient singular thermal stresses induced by crack.

The aim of this paper is to investigate transient thermal stresses in a hollow cylinder with a circumferential crack based on the generalized fractional thermoelasticity theory. The thermal stress intensity factors (SIFs) of embedded and surface cracks are determined. For a hollow cylinder subjected to heat shock at the surface, transient temperature field and thermal stresses are calculated using numerical inversion of the Laplace transform. The thermal stresses induced by crack along with the corresponding SIFs are obtained through the singular integral equation method. The influences of fractional order α and the phase lag of heat flux τ_q on the transient temperature, thermal stresses and thermal SIFs are analyzed for embedded and inner/outer surface cracks, respectively. Obtained numerical results are compared with those using the classical Fourier and hyperbolic heat conduction theories.

2. Formulation of the problem

Consider a hollow homogeneous isotropic thermoelastic cylinder with a circumferential crack, as shown in Fig. 1. The inner and outer radii of the cylinder are denoted as $r = a$ and $r = b$, respectively. The circumferential crack lies in the plane $z = 0$ and occupies the region $c < r < d$. Here we have used the cylindrical polar coordinate (r, θ, z). For simplicity, we consider an axisymmetric problem. Assume that initial temperature of the cylinder is T_0, the inner surface of the cylinder suffers a thermal shock T_a, and the outer surface is insulated. Then the boundary conditions can be expressed as

$$T(a,t) = T_a H(t), \tag{1}$$

$$\frac{\partial T(b,t)}{\partial r} = 0, \tag{2}$$

where $H(t)$ denotes the Heaviside unit step function. Under such

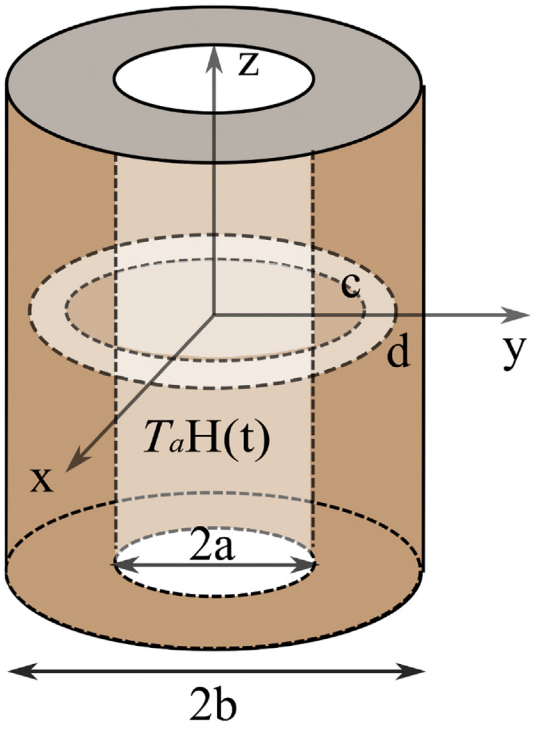

Fig. 1. A hollow cylinder containing a circumferential crack.

thermal shock, we will analyze transient thermal stress response due to the presence of a circumferential crack. For heat conduction problems, in the present paper a non-Fourier generalized fractional heat conduction law is adopted. Once transient temperature field is determined, thermal stresses induced by crack can be obtained by superposition under the assumption that crack and deformation do not change temperature distribution. Since singular thermal stresses are of particular interest, the corresponding thermal SIFs will be evaluated. Therefore, the problem is decomposed to two subproblems.

3. Thermal stresses in a hollow cylinder without crack

First, let us determine transient thermal stresses in a hollow cylinder without crack. To this end, it is sufficient to look for transient temperature in this cylinder subject to thermal shock. Applying fractional Taylor's series developed by Jumarie [30], we expand heat flux vector $\mathbf{q}(\mathbf{x}, t + \tau_q)$ up to fractional order α in phase lag time of heat flux τ_q to result in Refs. [31,32].

$$\mathbf{q}(\mathbf{x},t) + \frac{\tau_q^\alpha}{\alpha!}\frac{\partial^\alpha \mathbf{q}(\mathbf{x},t)}{\partial t^\alpha} = -k\nabla T(\mathbf{x}), \tag{3}$$

where k and T are thermal conductivity and absolute temperature, respectively, ∇ is the gradient operator, and the time-fractional differential operator $\partial^\alpha/\partial t^\alpha$ with $0 < \alpha \leq 1$ is defined by

$$\frac{\partial^\alpha f(*,t)}{\partial t^\alpha} = \begin{cases} f(*,t) - f(*,0), & \alpha \to 0 \\ I^{1-\alpha}\dfrac{\partial f(*,t)}{\partial t}, & 0 < \alpha < 1 \\ \dfrac{\partial f(*,t)}{\partial t}, & \alpha = 1, \end{cases} \tag{4}$$

with

$$I^{\alpha}f(*,t)=\frac{1}{\Gamma(\alpha)}\int_0^t(t-s)^{\alpha-1}f(*,s)ds,\quad \alpha>0. \tag{5}$$

In the above, $\Gamma(\alpha)$ is the Gamma function.

In combination with the conservation law of energy in terms of the heat conduction vector $\mathbf{q}$

$$\frac{\partial}{\partial t}(\rho_m c_p T)=-\nabla\cdot\mathbf{q}, \tag{6}$$

we get the desirable generalized fractional heat conduction equation

$$\rho_m c_p\frac{\partial T}{\partial t}+\frac{\tau_q^{\alpha}}{\alpha!}\frac{\partial^{\alpha}}{\partial t^{\alpha}}\left(\rho_m c_p\frac{\partial T}{\partial t}\right)=k\nabla^2 T \tag{7}$$

in which ρ_m and c_p are, respectively, mass density and specific heat, ∇^2 is the Laplacian operator. It is noted that if setting the phase lag time of heat flux $\tau_q\to 0$ or the fractional order $\alpha\to 0$, the above equation (7) reduces to the classical Fourier heat conduction equation, while the hyperbolic heat conduction equation is also recovered only setting the fractional order $\alpha=1$.

For a hollow cylinder, an axisymmetric problem of the generalized fractional heat conduction equation (7) becomes

$$k\left[\frac{1}{r}\frac{\partial}{\partial r}\left(r\frac{\partial T}{\partial r}\right)+\frac{\partial^2 T}{\partial z^2}\right]=\rho c_p\frac{\partial T}{\partial t}+\rho c_p\frac{\tau_q^{\alpha}}{\alpha!}\frac{\partial^{\alpha+1}T}{\partial t^{\alpha+1}}. \tag{8}$$

For convenience, introduce the following normalized parameters

$$\bar{r}=\frac{r}{b},\quad \bar{t}=\frac{tk}{\rho_m c_p b^2},\quad \bar{\tau}_q=\frac{\tau_q k}{\rho_m c_p b^2},\quad \theta=\frac{T-T_0}{T_a-T_0}. \tag{9}$$

In the following, we assume that the hollow cylinder is infinitely long, implying $\partial T/\partial z=0$. This is reasonable for enough long cylinders. Eq. (8) is then rewritten as

$$\frac{\partial^2\theta(\bar{r},\bar{t})}{\partial\bar{r}^2}+\frac{1}{\bar{r}}\frac{\partial\theta(\bar{r},\bar{t})}{\partial\bar{r}}=\frac{\partial\theta(\bar{r},\bar{t})}{\partial\bar{t}}+\frac{\bar{\tau}_q^{\alpha}}{\alpha!}\frac{\partial^{\alpha+1}\theta(\bar{r},\bar{t})}{\partial\bar{t}^{\alpha+1}} \tag{10}$$

subject to the following boundary and initial conditions

$$\theta(\bar{r}_{in},\bar{t})=H(\bar{t}),\quad \frac{\partial\theta(1,\bar{t})}{\partial\bar{r}}=0, \tag{11}$$

$$\theta(\bar{r},0)=0,\quad \frac{\partial\theta(\bar{r},0)}{\partial\bar{t}}=0, \tag{12}$$

where

$$\bar{r}_{in}=\frac{a}{b}. \tag{13}$$

Performing the Laplace transform with respect to time on the both sides of the generalized fractional heat conduction equation (10), we obtain

$$\frac{\partial^2}{\partial\bar{r}^2}\tilde{\theta}(\bar{r},s)+\frac{1}{\bar{r}}\frac{\partial}{\partial\bar{r}}\tilde{\theta}(\bar{r},s)=\left(s+\frac{\bar{\tau}_q^{\alpha}}{\alpha!}s^{\alpha+1}\right)\tilde{\theta}(\bar{r},s) \tag{14}$$

where s is the Laplace transform parameter, and a quantity with tilde over it denotes its Laplace transform. From Eq. (14), the temperature field in the Laplace transform domain can be expressed as

$$\tilde{\theta}(\bar{r},s)=A_1(s)I_0(\beta\bar{r})+A_2(s)K_0(\beta\bar{r}) \tag{15}$$

where $A_1(s)$ and $A_2(s)$ are two unknown functions which can be determined by the boundary conditions, I_0 and K_0 are the modified Bessel functions of the first and second kinds of purely imaginary argument, and

$$\beta=\sqrt{s+\frac{\bar{\tau}_q^{\alpha}}{\alpha!}s^{\alpha+1}}. \tag{16}$$

To determine $A_1(s)$ and $A_2(s)$, we employ the normalized forms of boundary conditions (11) in the Laplace domain

$$\tilde{\theta}(\bar{r}_{in},s)=\frac{1}{s},\quad \frac{\partial\tilde{\theta}(1,s)}{\partial\bar{r}}=0. \tag{17}$$

Inserting (17) into (15), after some algebra, leads to

$$A_1(s)=\frac{K_1(\beta)}{s[I_0(\beta\bar{r}_{in})K_1(\beta)+I_1(\beta)K_0(\beta\bar{r}_{in})]},\quad A_2(s)=\frac{I_1(\beta)}{s[I_0(\beta\bar{r}_{in})K_1(\beta)+I_1(\beta)K_0(\beta\bar{r}_{in})]}. \tag{18}$$

With these results in (18), the temperature field in the Laplace domain is obtained, and it in the time domain is readily determined by means of numerical inversion of the Laplace transform.

Owing to the fact that resultant axial force at any cross section vanishes, it requires

$$\int_a^b r\sigma_{zz}dr=0, \tag{19}$$

where the axial stress component σ_{zz} in an uncracked hollow cylinder is governed by the following equation [1].

$$\sigma_{zz}=\frac{2E\lambda}{(1-\nu)(b^2-a^2)}\int_a^b r(T-T_0)dr-\frac{E\lambda}{1-\nu}(T-T_0). \tag{20}$$

where E, ν and λ are the Young's modulus, Poisson's ratio, linear thermal expansion, respectively.

Now we introduce the following non-dimensional axial stress

$$\bar{\sigma}_{zz}=\frac{\sigma_{zz}(1-\nu)}{\lambda E(T_a-T_0)}, \tag{21}$$

and then the thermal stress component σ_{zz} can be rewritten in the Laplace domain as

$$\tilde{\sigma}_{zz}(\bar{r},s)=\frac{2}{1-\bar{r}_{in}^2}\int_{\bar{r}_{in}}^1\bar{r}\tilde{\theta}(\bar{r},s)dr-\tilde{\theta}(\bar{r},s). \tag{22}$$

Substituting Eq. (15) into Eq. (22) leads to

$$\tilde{\sigma}_{zz}(\bar{r},s)=\frac{2}{\beta\left(1-\bar{r}_{in}^2\right)}\{A_1[I_1(\beta)-\bar{r}_{in}I_1(\beta\bar{r}_{in})]+A_2[\bar{r}_{in}K_1(\beta\bar{r}_{in})-K_1(\beta)]\}-A_1I_0(\beta\bar{r})-A_2K_0(\beta\bar{r}). \tag{23}$$

The axial thermal stress response in the time domain can be immediately obtained by performing the inverse Laplace transform as follows:

$$\sigma_{zz}(\bar{r},\bar{t}) = \mathscr{L}^{-1}[\tilde{\sigma}_{zz}(\bar{r},s)] \triangleq p(\bar{r},\bar{t}). \tag{24}$$

4. Thermal stresses in a hollow cylinder with crack

With the thermal stress in an uncracked hollow cylinder at hand, in this section we determine the transient thermal stress in a hollow cylinder containing a circumferential crack. For this purpose the following non-dimensional displacement components and stress components along with non-dimensional coordinates are introduced

$$\bar{u} = \frac{u(1-\nu)}{\lambda(1+\nu)(T_a - T_0)b}, \quad \bar{w} = \frac{w(1-\nu)}{\lambda(1+\nu)(T_a - T_0)b}, \tag{25}$$

$$\bar{\sigma}_{rr} = \frac{\sigma_{rr}(1-\nu)}{\lambda E(T_a - T_0)}, \quad \bar{\sigma}_{rz} = \frac{\sigma_{rz}(1-\nu)}{\lambda E(T_a - T_0)}, \tag{26}$$

$$\bar{z} = \frac{z}{b}, \quad \bar{c} = \frac{c}{b}, \quad \bar{d} = \frac{d}{b} \tag{27}$$

where u and w are the radial and axial displacement components, respectively; σ_{rr} and σ_{rz} stand for the normal and shear stress components.

Since transient thermal stresses have been derived in the foregoing section, in order to determine singular thermal stresses disturbed by crack, it is sufficient to a crack problem by superposition. In other words, due to the assumption of traction-free crack surfaces, we only solve a perturbation problem for a cracked cylinder where the negative of resulting thermal stress $p(\bar{r},\bar{t})$ given in Eq. (24) is exerted at the crack surfaces. Consideration of symmetry allows us to only analyze one half of the cylinder, i.e. $z \geq 0$, and then the non-dimensional boundary conditions for a mode I crack can be written below

$$\bar{\sigma}_{rr}(1,\bar{z},\bar{t}) = 0, \qquad 0 \leq \bar{z} \leq \infty \tag{28}$$

$$\bar{\sigma}_{rz}(1,\bar{z},\bar{t}) = 0, \qquad 0 \leq \bar{z} \leq \infty \tag{29}$$

$$\bar{\sigma}_{rr}(\bar{r}_{in},\bar{z},\bar{t}) = 0, \quad 0 \leq \bar{z} \leq \infty \tag{30}$$

$$\bar{\sigma}_{rz}(\bar{r}_{in},\bar{z},\bar{t}) = 0, \quad 0 \leq \bar{z} \leq \infty \tag{31}$$

$$\bar{\sigma}_{rz}(\bar{r},0,\bar{t}) = 0, \qquad \bar{r}_{in} \leq \bar{r} \leq 1 \tag{32}$$

$$u(\bar{r},0,\bar{t}) = 0, \qquad \bar{r}_{in} \leq \bar{r} < \bar{c}, \ \ \bar{d} < \bar{r} \leq 1 \tag{33}$$

$$\bar{\sigma}_{zz}(\bar{r},0,\bar{t}) = -p(\bar{r},\bar{t}), \qquad \bar{c} < \bar{r} < \bar{d}. \tag{34}$$

For axisymmetric elastic problems of an isotropic hollow cylinder, the non-dimensional governing equation, displacement components, and stress components are expressed in terms of the Love potential function $\Phi(r,z,t)$ as

$$\bar{u} = -\frac{\partial^2 \bar{\Phi}}{\partial \bar{r} \partial \bar{z}}, \tag{35}$$

$$\bar{w} = 2(1-\nu)\nabla^2 \bar{\Phi} - \frac{\partial^2 \bar{\Phi}}{\partial \bar{z}^2}, \tag{36}$$

$$\bar{\sigma}_{rr} = \frac{\partial}{\partial \bar{z}}\left(\nu \nabla^2 \bar{\Phi} - \frac{\partial^2 \bar{\Phi}}{\partial \bar{r}^2}\right), \tag{37}$$

$$\bar{\sigma}_{zz} = \frac{\partial}{\partial \bar{z}}\left[(2-\nu)\nabla^2 \bar{\Phi} - \frac{\partial^2 \bar{\Phi}}{\partial \bar{z}^2}\right], \tag{38}$$

$$\bar{\sigma}_{rz} = \frac{\partial}{\partial \bar{r}}\left[(1-\nu)\nabla^2 \bar{\Phi} - \frac{\partial^2 \bar{\Phi}}{\partial \bar{z}^2}\right], \tag{39}$$

where ∇^2 denotes the Laplacian operator in cylindrical coordinates

$$\nabla^2 = \frac{\partial^2}{\partial \bar{r}^2} + \frac{1}{\bar{r}}\frac{\partial}{\partial \bar{r}} + \frac{\partial^2}{\partial \bar{z}^2} \tag{40}$$

and $\bar{\Phi}(\bar{r},\bar{z},\bar{t})$ is a non-dimensional Love potential function $\bar{\Phi}(\bar{r},\bar{z},\bar{t})$ defined by

$$\bar{\Phi}(\bar{r},\bar{z},\bar{t}) = \frac{\Phi(r,z,t)(1-\nu)}{\lambda E(T_a - T_0)b^3}, \tag{41}$$

and satisfies the following bi-harmonic equation

$$\nabla^2 \nabla^2 \bar{\Phi}(\bar{r},\bar{z},\bar{t}) = 0. \tag{42}$$

Solving the bi-harmonic equation (42) and making use of the regular condition of the stresses at infinity, one gets the desired bi-harmonic function $\bar{\Phi}(\bar{r},\bar{z},\bar{t})$ in the form

$$\begin{aligned}\bar{\Phi} = \frac{2}{\pi}\int_0^\infty &[C_1 I_0(\xi\bar{r}) + C_2 K_0(\xi\bar{r}) + \bar{r}C_3 I_1(\xi\bar{r}) + \bar{r}C_4 K_1(\xi\bar{r})] \ \sin(\xi\bar{z})d\xi \\ + \int_0^\infty &\zeta(C_5 + C_6\bar{z})\exp(-\zeta\bar{z})J_0(\zeta\bar{r})d\zeta\end{aligned} \tag{43}$$

where C_i $(i = 1,\ldots 6)$'s are unknown functions in ξ to be determined from the boundary conditions (28)–(34). To determine them, it is convenient to first give expressions for displacements and stresses, which are immediately obtained through substituting Eq. (43) into Eqs. (35)–(39)

$$\begin{aligned}\bar{u}(\bar{r},\bar{z},\bar{t}) = -\frac{2}{\pi}\int_0^\infty &\xi^2[C_1 I_1(\xi\bar{r}) - C_2 K_1(\xi\bar{r}) + \bar{r}C_3 I_0(\xi\bar{r}) \\ &-\bar{r}C_4 K_0(\xi\bar{r})] \ \cos(\xi\bar{z})d\xi \\ + \int_0^\infty &\zeta^2[C_6 - \zeta(C_5 + C_6\bar{z})]\exp(-\zeta\bar{z})J_1(\zeta\bar{r})d\zeta\end{aligned} \tag{44}$$

$$\overline{w}(\overline{r},\overline{z},\overline{t}) = \frac{2}{\pi}\int_0^\infty \xi\{C_1\xi I_0(\xi\overline{r}) + C_2\xi K_0(\xi\overline{r}) + C_3[4(1-\nu)I_0(\xi\overline{r}) + \xi\overline{r}I_1(\xi\overline{r})] - C_4[4(1-\nu)K_0(\xi\overline{r}) + \xi\overline{r}K_1(\xi\overline{r})]\}\sin(\xi\overline{z})d\xi + \int_o^\infty \zeta^2[2(2\nu-1)C_6 - \zeta(C_5 + C_6\overline{z})]\exp(-\zeta\overline{z})J_0(\zeta\overline{r})d\zeta \tag{45}$$

$$\begin{aligned}\overline{\sigma}_{rr}(\overline{r},\overline{z},\overline{t}) = \frac{2}{\pi}\int_0^\infty \xi^2\{C_1[-\xi I_0(\xi\overline{r}) + \frac{I_1(\xi\overline{r})}{\overline{r}}] \\ + C_3[(2\nu-1)I_0(\xi\overline{r}) - \xi\overline{r}I_1(\xi\overline{r})] - C_2[\xi K_0(\xi\overline{r}) + \frac{K_1(\xi\overline{r})}{\overline{r}}] \\ - C_4[(2\nu-1)K_0(\xi\overline{r}) + \xi\overline{r}K_1(\xi\overline{r})]\}\cos(\xi\overline{z})d\xi \\ - \int_0^\infty \frac{\zeta^2}{\overline{r}}[C_6 - \zeta(C_5 + C_6\overline{z})]\exp(-\zeta\overline{z})J_1(\zeta\overline{r})d\zeta \\ + \int_0^\infty \zeta^3[(1+2\nu)C_6 - \zeta(C_5 + C_6\overline{z})]\exp(-\zeta\overline{z})J_0(\zeta\overline{r})d\zeta\end{aligned} \tag{46}$$

$$\begin{aligned}\overline{\sigma}_{zz}(\overline{r},\overline{z},\overline{t}) = \frac{2}{\pi}\int_0^\infty \xi^2\{C_1\xi I_0(\xi\overline{r}) + C_2\xi K_0(\xi\overline{r}) - C_3[(2\nu-4)I_0(\xi\overline{r}) \\ - \xi\overline{r}I_1(\xi\overline{r})] + C_4[(2\nu-4)K_0(\xi\overline{r}) + \xi\overline{r}K_1(\xi\overline{r})]\}\cos(\xi\overline{z})d\xi \\ + \int_0^\infty \zeta^3[(1-2\nu)C_6 + \zeta(C_5 + C_6\overline{z})]\exp(-\zeta\overline{z})J_0(\zeta\overline{r})d\zeta\end{aligned} \tag{47}$$

$$\begin{aligned}\overline{\sigma}_{rz}(\overline{r},\overline{z},\overline{t}) = \frac{2}{\pi}\int_0^\infty \xi^2\{C_1\xi I_0(\xi\overline{r}) - C_2\xi K_1(\xi\overline{r}) - C_3[(2\nu-2)I_1(\xi\overline{r}) \\ - \xi\overline{r}I_0(\xi\overline{r})] - C_4[(2\nu-2)K_1(\xi\overline{r}) + \xi\overline{r}K_0(\xi\overline{r})]\}\sin(\xi\overline{z})d\xi \\ + \int_0^\infty \zeta^3[-2\nu C_6 + \zeta(C_5 + C_6\overline{z})]\exp(-\zeta\overline{z})J_1(\zeta\overline{r})d\zeta.\end{aligned} \tag{48}$$

The above boundary-value problem may be reduced to a singular integral equation by introducing a new function ψ, defined by

$$\frac{d}{d\overline{r}}\overline{w}(\overline{r},0,\overline{t}) = \psi(\overline{r},\overline{t}). \tag{49}$$

Considering the displacement boundary condition (33), $\psi(\overline{r},\overline{t})$ should satisfy the single value condition below:

$$\int_{\overline{c}}^{\overline{d}} \psi(\overline{r},\overline{t})d\overline{r} = 0. \tag{50}$$

In order to determine the unknown function $\psi(\overline{r},\overline{t})$, we substitute Eq. (47) into (34), and after lengthy manipulation, finally get the following singular integral equation with Cauchy kernel

$$\frac{1}{\pi}\int_{\overline{c}}^{\overline{d}} \psi(\overline{r}_0,\overline{t})\left[\frac{1}{\overline{r}_0 - \overline{r}} + L(\overline{r},\overline{r}_0) + 2\overline{r}_0\int_0^\infty M(\overline{r},\overline{r}_0,\xi)d\xi\right]d\overline{r}_0 = -2(1-\nu)p(\overline{r},\overline{t}),\ \overline{c} < \overline{r} < \overline{d} \tag{51}$$

in which

$$\begin{aligned}M(\overline{r},\overline{r}_0,\xi) = \frac{\xi^2}{\Delta}\{\xi I_0(\xi\overline{r})\Delta_1 + \xi K_0(\xi\overline{r})\Delta_2 + [(4-2\nu)I_0(\xi\overline{r}) \\ + \xi\overline{r}I_1(\xi\overline{r})]\Delta_3\} \\ + \{[(2\nu-4)K_0(\xi\overline{r}) + \xi\overline{r}K_1(\xi\overline{r})]\Delta_4\}\end{aligned} \tag{52}$$

$$L(\overline{r},\overline{r}_0) = \frac{m(\overline{r},\overline{r}_0) - 1}{\overline{r}_0 - \overline{r}} + \frac{m(\overline{r},\overline{r}_0)}{\overline{r}_0 + \overline{r}} \tag{53}$$

and

$$m(\overline{r},\overline{r}_0) = \begin{cases} E\left(\frac{\overline{r}}{\overline{r}_0}\right), \overline{r} < \overline{r}_0 \\ \frac{\overline{r}}{\overline{r}_0}E\left(\frac{\overline{r}_0}{\overline{r}}\right) + \frac{\overline{r}_0^2 - \overline{r}^2}{\overline{r}_0\overline{r}}K\left(\frac{\overline{r}_0}{\overline{r}}\right), \overline{r} > \overline{r}_0. \end{cases} \tag{54}$$

In the above equation, $K(*)$ and $E(*)$ are the complete elliptic integrals of the first and second kind, respectively, and Δ_j $(i,j = 1,2,3,4)$ and Δ are given in Appendix A.

By introducing the following normalized parameters,

$$\overline{r} = \frac{\overline{d} - \overline{c}}{2}\rho + \frac{\overline{d} + \overline{c}}{2} \tag{55}$$

$$\overline{r}_0 = \frac{\overline{d} - \overline{c}}{2}\rho_0 + \frac{\overline{d} + \overline{c}}{2} \tag{56}$$

where $-1 < \rho, \rho_0 < 1$, the singular integral Eq. (51) and the single value condition (50) could be rewritten as,

$$\frac{1}{\pi}\int_{-1}^{1} \Psi(\rho_0,\overline{t})\left[\frac{1}{\rho_0 - \rho} + \overline{L}^*(\rho,\rho_0)\right]d\rho_0 = -2(1-\nu)\overline{p}(\rho,\overline{t}),\ \left|\rho\right| < 1 \tag{57}$$

$$\int_{-1}^{1} \Psi(\rho_0,t)d\rho_0 = 0, \tag{58}$$

in which

$$\Psi(\rho_0,\overline{t}) = \psi(\overline{r}_0,\overline{t}) \tag{59}$$

$$\overline{L}^*(\rho,\rho_0) = \overline{L}(\rho,\rho_0) + \left[\left(\overline{d} - \overline{c}\right)\rho_0 + \overline{d} + \overline{c}\right]\int_0^\infty \overline{M}(\rho,\rho_0,\xi)d\xi \tag{60}$$

$$\overline{p}(\rho,\overline{t}) = p(\overline{r},\overline{t}) \tag{61}$$

with

$$\overline{L}(\rho,\rho_0)=\frac{\overline{d}-\overline{c}}{2}L(\overline{r},\overline{r}_0), \tag{62}$$

$$\overline{M}(\rho,\rho_0,\xi)=\frac{\overline{d}-\overline{c}}{2}M(\overline{r},\overline{r}_0,\xi). \tag{63}$$

An appropriate solution of (57) may be of the form

$$\Psi(\rho_0,\overline{t})=f(\rho_0,\overline{t})(1+\rho_0)^{\varpi_1}(1-\rho_0)^{\varpi_2},\quad -1<\rho_0<1, \tag{64}$$

and the singular integral Eq. (57) is solved using the well-known numerical quadrature formulas [33].

4.1. Embedded crack

For an embedded internal crack with $\overline{r}_{in}<\overline{c}<\overline{d}<1$, the Cauchy kernel $1/(\rho_0-\rho)$ is the dominant kernel and the power-law exponents are found to be $\varpi_1=\varpi_2=-1/2$ since the thermal stresses at the crack fronts $\overline{r}=\overline{c},\overline{d}$ exhibit singular behavior. In this case, by employing the Lobatto–Chebyshev quadrature formula [34] of the closed-form

$$\frac{1}{\pi}\int_{-1}^{1}\frac{f(\rho_0,\overline{t})}{(\rho_0-\rho)\sqrt{1-\rho_0^2}}d\rho_0=\frac{1}{n}\sum_{k=0}^{n}\gamma_k\frac{f(\rho_{0k},\overline{t})}{\rho_{0k}-\rho_l}, \tag{65}$$

one finds that Eqs. (57) and (58) can be approximated by the following system of $n+1$ linear algebraic equations in $n+1$ unknown discrete points of $f(\rho_{0k},\overline{t})$

$$\frac{1}{n}\sum_{k=0}^{n}\gamma_k f(\rho_{0k},\overline{t})\left[\frac{1}{\rho_{0k}-\rho_l}+\overline{L}^*(\rho_l,\rho_{0k})\right]=-2(1-\nu)\overline{p}(\rho_l,\overline{t}),l=1,2,\ldots,n \tag{66}$$

$$\sum_{k=0}^{n}\frac{\gamma_k}{n}f(\rho_{0k},\overline{t})=0, \tag{67}$$

where

$$\rho_{0k}=\cos\left(\frac{k}{n}\pi\right),\ k=0,1,2,\ldots n, \tag{68}$$

$$\rho_l=\cos\left(\frac{2l-1}{2n}\pi\right),\ l=1,2,\ldots n, \tag{69}$$

$$\gamma_0=\gamma_n=\frac{1}{2},\quad \gamma_1=\gamma_2=\ldots=\gamma_{n-1}=1. \tag{70}$$

This method has a remarkable advantage as compared to the Gauss–Chebyshev quadrature formula [33], since the thermal SIFs at the crack fronts are calculated directly for the former, and evaluated with a complementary procedure such as extrapolation based on the determined internal values for the latter.

Solving the above resulting system gives the values of $f(\rho_{0k},\overline{t})$ at all positions ρ_{0k}. Of particular importance are the values of $f(\pm1,\overline{t})$ at the crack fronts, since they are exactly proportional to the thermal SIFs near the crack fronts. In fact, taking into account

$$\frac{1}{\pi}\int_{-1}^{1}\frac{1}{\sqrt{1-\rho_0^2}}\frac{1}{\rho_0-z}d\rho_0=-\frac{1}{\sqrt{z^2-1}},\quad z\notin[-1,1], \tag{71}$$

where z is a complex point lying in the complex plane cut along the segment $[-1,1]$, and the branch $\sqrt{z^2-1}$ takes positive when z takes a real number larger than 1, we have the axial thermal stress near crack fronts

$$\overline{\sigma}_{zz}(\rho,0,\overline{t})=\frac{1}{2\pi(1-\nu)}\int_{-1}^{1}\Psi(\rho_0,\overline{t})\left[\frac{1}{\rho_0-\rho}+\overline{L}^*(\rho,\rho_0)\right]d\rho_0$$
$$=\frac{-\rho f(\pm1,\overline{t})}{2(1-\nu)\sqrt{\rho^2-1}}+O(1),\quad \rho>1 \text{ or } \rho<-1. \tag{72}$$

According to the thermal SIFs, defined by

$$K_I^{in}(\overline{t})=\lim_{r\to c-0}\sqrt{2(c-r)}\sigma_{zz}(r,0,\overline{t}),\ \text{inner crack front}, \tag{73}$$

$$K_I^{out}(\overline{t})=\lim_{r\to d+0}\sqrt{2(r-d)}\sigma_{zz}(r,0,\overline{t}),\ \text{outer crack front}, \tag{74}$$

we obtain

$$\overline{K}_I^{in}(\overline{t})=\frac{f(-1,\overline{t})}{2(1-\nu)}\sqrt{\frac{\overline{d}-\overline{c}}{2}}, \tag{75}$$

$$\overline{K}_I^{out}(\overline{t})=-\frac{f(1,\overline{t})}{2(1-\nu)}\sqrt{\frac{\overline{d}-\overline{c}}{2}}, \tag{76}$$

where the normalized thermal SIF is defined by

$$\overline{K}_I=\frac{(1-\nu)K_I}{\lambda E(T_a-T_0)\sqrt{b}}. \tag{77}$$

4.2. Outer surface crack

Now we turn our attention to outer and inner circumferential surface cracks. Here in this subsection, an outer surface crack with $\overline{r}_{in}<\overline{c}<\overline{d}=1$ is focused. For this case, the singular integral equation (57) is still valid, while the single value condition (58) is no longer needed since the surface crack has only one crack front $r=c$, i.e the crack front $r=d$ disappears. Under such circumstances, after a lengthy analysis, we decompose the function $M(\overline{r},\overline{r}_0,\xi)$ into two parts, namely

$$\overline{M}(\overline{r},\overline{r}_0,\xi)=M_\infty(\overline{r},\overline{r}_0,\xi)+\Delta M(\overline{r},\overline{r}_0,\xi) \tag{78}$$

where

$$M_\infty(\overline{r},\overline{r}_0,\xi)=-\frac{1}{2\sqrt{\overline{r}\,\overline{r}_0}}\Big[2\xi^2(1-\overline{r})(1-\overline{r}_0)-3\xi(1-\overline{r}_0)-\xi(1-\overline{r})+2\Big]\exp[-\xi(2-\overline{r}-\overline{r}_0)]. \tag{79}$$

It is easily found that

$$\int_0^\infty M_\infty(\bar{r},\bar{r}_0,\xi)d\xi = \frac{1}{2\sqrt{\bar{r}\,\bar{r}_0}}\left[\frac{1}{2-\bar{r}-\bar{r}_0} - \frac{6(1-\bar{r})}{(2-\bar{r}-\bar{r}_0)^2} + \frac{4(1-\bar{r})^2}{(2-\bar{r}-\bar{r}_0)^3}\right] \triangleq W(\bar{r},\bar{r}_0), \tag{80}$$

and $\Delta M(\bar{r},\bar{r}_0,\xi)$ has a rapid convergence as ξ approaches to infinity. Therefore, Eq. (57) can be rewritten as

$$\frac{1}{\pi}\int_{-1}^{1}\Psi(\rho_0,\bar{t})\left[\frac{1}{\rho_0-\rho}+\bar{L}^*(\rho,\rho_0)\right]d\rho_0 = -2(1-\nu)\bar{p}(\rho,\bar{t}) \tag{81}$$

in which

$$\bar{L}^*(\rho,\rho_0) = \bar{L}(\rho,\rho_0) + \left[\left(\bar{d}-\bar{c}\right)\rho_0+\bar{d}+\bar{c}\right]\bar{W}(\rho,\rho_0) + \left[\left(\bar{d}-\bar{c}\right)\rho_0+\bar{d}+\bar{c}\right]\int_0^\infty\left[\bar{M}(\rho,\rho_0,\xi)-\bar{M}_\infty(\rho,\rho_0,\xi)\right]d\xi \tag{82}$$

$$\bar{M}_\infty(\rho,\rho_0,\xi) = \frac{\bar{d}-\bar{c}}{2}M_\infty(\bar{r},\bar{r}_0,\xi), \tag{83}$$

$$\bar{W}(\rho,\rho_0) = \frac{\bar{d}-\bar{c}}{2}W(\bar{r},\bar{r}_0). \tag{84}$$

For an outer surface crack, the singularity indices must satisfy $\varpi_1 = -\varpi_2 = -1/2$. Applying the Gauss–Jacobi quadrature formula [33].

$$\frac{1}{\pi}\int_{-1}^{1}\left(\frac{1-\rho_0}{1+\rho_0}\right)^{1/2}\frac{f(\rho_0,\bar{t})}{\rho_0-\rho}d\rho_0 = \sum_{k=1}^{n}\frac{2(1-\rho_{0k})}{2n+1}\frac{f(\rho_{0k},\bar{t})}{\rho_{0k}-\rho_l}, \tag{85}$$

where

$$\rho_{0k} = \cos\left(\frac{2k}{2n+1}\pi\right),\ k=1,2,\ldots n, \tag{86}$$

$$\rho_l = \cos\left(\frac{2l-1}{2n+1}\pi\right),\ l=1,2,\ldots n, \tag{87}$$

from (57) one gets a system of linear algebraic equations in n collocation points

$$\sum_{k=1}^{n}\frac{1-\rho_{0k}}{2n+1}f(\rho_{0k},\bar{t})\left[\frac{1}{\rho_{0k}-\rho_l}+\bar{L}^*(\rho_l,\rho_{0k})\right] = -(1-\nu)\bar{p}(\rho_l,\bar{t}). \tag{88}$$

Similar to the case of an embedded crack, the dimensionless thermal SIFs at the crack front of an outer surface crack can be expressed as

$$\bar{K}_I^c(\bar{t}) = \frac{f(-1,\bar{t})}{2(1-\nu)}\sqrt{2(1-\bar{c})}. \tag{89}$$

and $f(-1,\bar{t})$ can be obtained from $f(\rho_{0k},\bar{t})$ using the interpolation formulas given in Ref. [35].

4.3. Inner surface crack

For an inner surface circumferential crack with $\bar{r}_{in} = \bar{c} < \bar{d} < 1$, an analogous treatment to the above for an outer surface crack is done. In this case, the singularity indices must satisfy $-\varpi_1 = \varpi_2 = -1/2$. By asymptotic analysis of $M(\bar{r},\bar{r}_0,\xi)$, one has a similar function $M_\infty(\bar{r},\bar{r}_0,\xi)$ whose integral is unbounded $W(\bar{r},\bar{r}_0)$ as $\bar{r}$ and $\bar{r}_0$ approach the end point $\bar{c} = \bar{r}_{in}$

$$M_\infty(\bar{r},\bar{r}_0,\xi) = \frac{1}{2\sqrt{\bar{r}\,\bar{r}_0}}\left[2\xi^2(\bar{r}-\bar{r}_{in})(\bar{r}_0-\bar{r}_{in}) - 3\xi(\bar{r}_0-\bar{r}_{in}) - \xi(\bar{r}-\bar{r}_{in}) + 2\right]\exp[-\xi(\bar{r}+\bar{r}_0-2\bar{r}_{in})] \tag{90}$$

instead of M_∞ in (79), and

$$\int_0^\infty M_\infty(\bar{r},\bar{r}_0,\xi)d\xi = \frac{1}{2\sqrt{\bar{r}\,\bar{r}_0}}\left[\frac{-1}{\bar{r}+\bar{r}_0-2\bar{r}_{in}} + \frac{6(\bar{r}-\bar{r}_{in})}{(\bar{r}+\bar{r}_0-2\bar{r}_{in})^2} - \frac{4(\bar{r}-\bar{r}_{in})^2}{(\bar{r}+\bar{r}_0-2\bar{r}_{in})^3}\right] \triangleq W(\bar{r},\bar{r}_0), \tag{91}$$

instead of the integral in (80).

Considering the quadrature formula

$$\frac{1}{\pi}\int_{-1}^{1}\left(\frac{1+\rho_0}{1-\rho_0}\right)^{1/2}\frac{f(\rho_0,\bar{t})}{\rho_0-\rho}d\rho_0 = \sum_{k=1}^{n}\frac{2(1+\rho_{0k})}{2n+1}\frac{f(\rho_{0k},\bar{t})}{\rho_{0k}-\rho_l} \tag{92}$$

where

$$\rho_{0k} = \cos\left(\frac{2k-1}{2n+1}\pi\right),\ k=1,2,\ldots n, \tag{93}$$

$$\rho_l = \cos\left(\frac{2l}{2n+1}\pi\right),\ l=1,2,\ldots n, \tag{94}$$

from (57) one gets the following system of algebraic equations

$$\sum_{k=1}^{n}\frac{1+\rho_{0k}}{2n+1}f(\rho_{0k},\bar{t})\left[\frac{1}{\rho_{0k}-\rho_l}+\bar{L}^*(\rho_l,\rho_{0k})\right]d\xi = -(1-\nu)\bar{p}(\rho_l,\bar{t}). \tag{95}$$

The thermal SIF at the crack front of an inner surface crack can be expressed in the dimensionless form as

$$\bar{K}_I^d(\bar{t}) = \frac{-f(1,\bar{t})}{2(1-\nu)}\sqrt{2\left(\bar{d}-\bar{r}_{in}\right)}$$

and $f(1,\bar{t})$ can be obtained from $f(\rho_{0k},\bar{t})$ using the interpolation formulas given in Ref. [35].

5. Numerical results and discussion

In this section, numerical computations are carried out to show the effects of phase lag of heat flux $\bar{\tau}_q$, fractional order α and crack geometry size on the transient temperature field, thermal axial stress, and the thermal SIFs for three different kinds of crack in a hollow cylinder. Here we choose the non-dimensional inner radius of a hollow cylinder as $\bar{r}_{in} = 0.5$ and Poisson's' ratio as $\nu = 0.32$.

The temperature field and axial thermal stress in the time domain can be obtained from the Laplace transform domain by using the numerical inversion technique of the Laplace transform described in Ref. [36]. According to [36], the numerical inversion of the Laplace transform of a function, $\bar{f}(\eta,s)$, at time $\xi_j = jT_{total}/N$ is

achieved by the following sum of series

$$f(\eta,\xi_j)=\frac{2e^{a\xi_j}}{T_{total}}\mathrm{Re}\left\{-\frac{1}{2}\tilde{f}(\eta,a)+\sum_{k=0}^{N-1}[A(\eta,k)+iB(\eta,k)]e^{i2\pi jk/N}\right\},\quad j=0,1,2,\ldots,N-1 \tag{96}$$

where $i=\sqrt{-1}$ and

$$A(\eta,k)=\sum_{l=0}^{L}\mathrm{Re}\,\tilde{f}\left[\eta,a+\frac{i2\pi(k+lN)}{T_{total}}\right], \tag{97}$$

$$B(\eta,k)=\sum_{l=0}^{L}\mathrm{Im}\,\tilde{f}\left[\eta,a+\frac{i2\pi(k+lN)}{T_{total}}\right]. \tag{98}$$

In the above, Re and Im denote real and imaginary parts of a complex function, respectively, an arbitrary real number a should be greater than all of the real parts of the function's singularity points, and T_{total} is the total time over which the numerical inversion is performed. Adopting the method, the accuracy of numerical inversion of the Laplace transform is influenced by choice of parameters L and N; in the present paper, aT_{total} and LN are chosen as 6 and 600, respectively, unless otherwise stated.

Firstly, the transient normalized temperature field θ as a function of non-dimensional time $\bar{t}$ at a given location $\bar{r}=0.6$ for different fractional orders α is shown in Fig. 2. It should be noted that the fractional heat conduction model reduces to the classical Fourier heat conduction model if setting $\alpha=0$ and the hyperbolic heat conduction if setting $\alpha=1$. Clearly, with the fractional order α rising, wave-like oscillation behavior becomes more evident besides diffusion characteristic. In particular, the transient temperature change contains the contribution of reflected waves due to the surface for the case of $\alpha=1$; then the temperature change curve with $\alpha=1$ exhibits sharp jumps at certain positions. At initial time, the temperature remains unchanged since heat waves do not arrive at location $\bar{r}=0.6$. After some time, temperature has a rapid climb with arrival of heat waves. Those jump positions just correspond to the time period during which waves travel from the reflected surfaces. Note that not normal sinusoidal oscillation waves are observed in Fig. 2, since the temperature change is not merely complete wave behavior, and but diffusion is also included. A similar fluctuation trend can be found from Fig. 3 in Ref. [17].

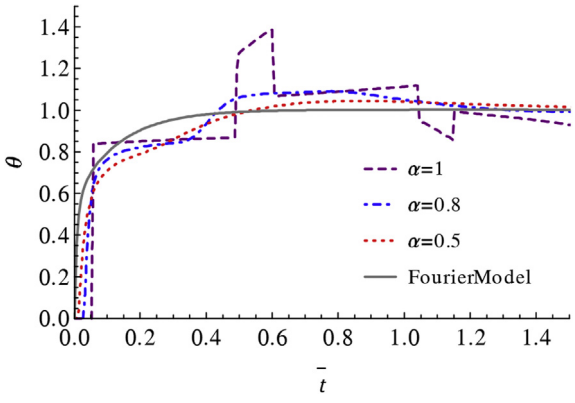

Fig. 2. The evolution of temperature change at a location $\bar{r}=0.6$ with as a function of the normalized time in a hollow cylinder with $\bar{r}_{in}=0.5$ subject to heat shock for $\alpha=0, 0.5, 0.8, 1$ and $\bar{\tau}_q=0.3$.

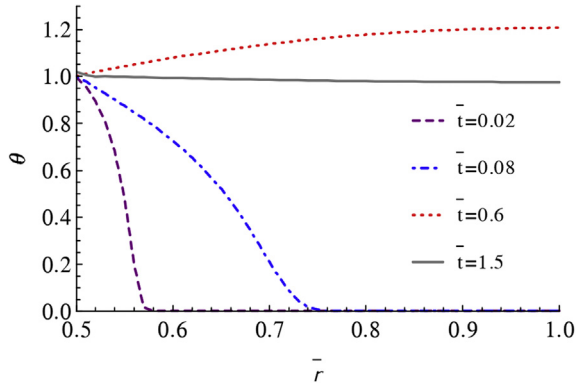

Fig. 3. The temperature distribution in a hollow cylinder with $\bar{r}_{in}=0.5$, $\alpha=0.8$ and $\bar{\tau}_q=0.3$ for various normalized times.

In Fig. 3, the transient temperature change in the hollow cylinder is shown for different normalized time periods with $\alpha=0.8$ and $\bar{\tau}_q=0.3$. At $\bar{t}=0.02$ and $\bar{t}=0.08$, heat diffusion-waves travel from the inner surface towards to the outer surface with a finite propagation speed. Then heat diffusion-waves arrive the outer surface at certain time less than $\bar{t}=0.6$ and are reflected back towards the inner surface. Finally, the temperature change tends to be steady at $\bar{t}=1.5$ after a period of back and forth travelling. In other words, wave behavior prevails over diffusion during the stage of beginning, and diffusion has a dominating role after some period.

The influence of the phase lag of heat flux $\bar{\tau}_q$ is examined in the following. The transient normalized temperature field θ at arbitrary spatial locations at time $\bar{t}=0.06$ is illustrated for various values of the phase lag of heat flux $\bar{\tau}_q$ in Fig. 4. It should be noted that the classical Fourier heat conduction model is recovered from the present with $\bar{\tau}_q=0$. It is seen that at $\bar{t}=0.06$, the temperature change at arbitrary location is immediately responded for the classical Fourier heat conduction model, as expected, whereas it is not immediately caused for those locations away from the inner surface for $\alpha\neq0$. This implies the influence of phase lag of heat flux. From Fig. 4, it is seen that the influences of phase lag of heat flux $\bar{\tau}_q$ strongly depends on the fractional order α. For example, for same phase lag of non-dimensional heat flux $\bar{\tau}_q=0.25$ in Fig. 4, the temperature change with different fractional orders has a striking difference, and has a sharp jump for the hyperbolic model with $\alpha=1$. This phenomenon is in line with that indicated in Ref. [11].

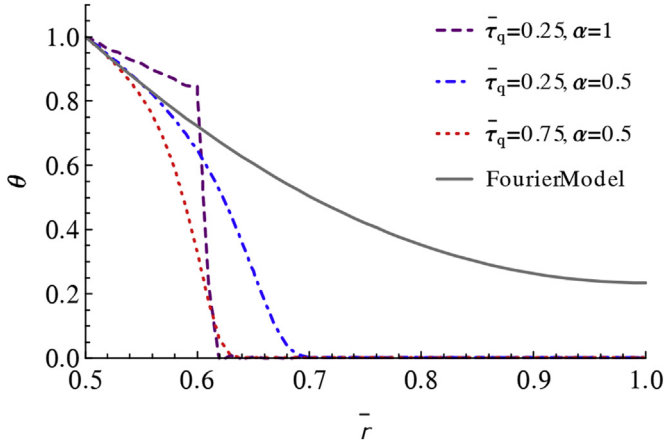

Fig. 4. The influence of phase lag of heat flux $\bar{\tau}_q$ on temperature distribution in a hollow cylinder with $\bar{r}_{in}=0.5$ at the normalized time $\bar{t}=0.06$.

Nevertheless, the temperature change curve for $\alpha = 0.5$ exhibits a smooth drop.

With the above-obtained temperature change in a hollow cylinder, the response evolution of the non-dimensional axial thermal stress $\bar{\sigma}_{zz}$ at location $\bar{r} = 0.6$ as a function of non-dimensional time $\bar{t}$ is depicted in Fig. 5. In what follows, we analyze the case of hot shock $T_a > T_0$, and for cold shock ($T_a < T_0$), transient axial thermal stress at arbitrary location of the cylinder merely alters its sign in same magnitude due to the cooling condition. For hot shock $T_a > T_0$, the axial thermal stress may be either compressive or tensile depending on time. For the classical Fourier heat conduction model the axial thermal stress at location $\bar{r} = 0.6$ is always compressive, while compressive or tensile thermal stress is exhibited in an alternative way for fractional heat conduction model. This feature is particularly obvious for hyperbolic heat conduction model with $\alpha = 1$.

The response evolution of the non-dimensional axial thermal stress $\bar{\sigma}_{zz}$ in a hollow cylinder with $\alpha = 0.8$ and $\bar{\tau}_q = 0.3$ is presented for different normalized time periods in Fig. 6. In Fig. 6, the axial thermal stress near the inner surface at first is compressive, while it in the region close to the outer surface is tensile. After some period, transient compressive stress near the inner surface gradually becomes tensile, while the region near the outer surface experiences from tensile state to compressive state. This is attributed to the fact that thermal shock reflecting from the outer surface affects the stresses and changes their signs.

Fig. 7 shows the influence of phase lag of heat flux $\bar{\tau}_q$ on the axial thermal stress response in a hollow cylinder when $\bar{t} = 0.06$.

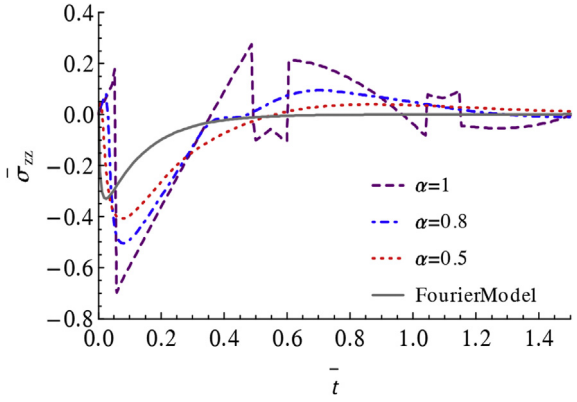

Fig. 5. The effects of fractional order α on the transient axial thermal stress history in a hollow cylinder with $\bar{r}_{in} = 0.5$ at location $\bar{r} = 0.6$ and $\bar{\tau}_q = 0.3$.

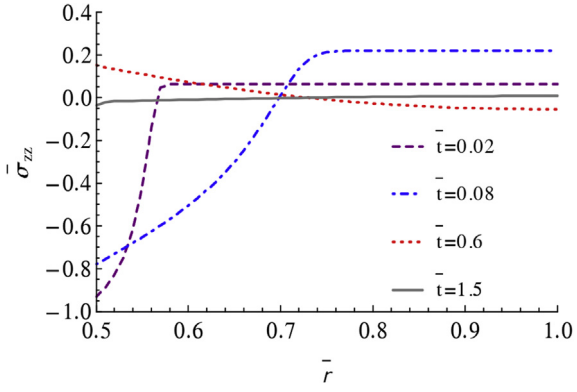

Fig. 6. The transient axial thermal stress distribution in a hollow cylinder with $\bar{r}_{in} = 0.5$, $\alpha = 0.8$, $\bar{\tau}_q = 0.3$ for various normalized times.

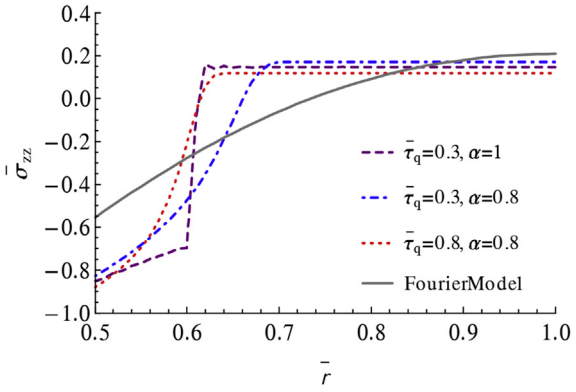

Fig. 7. The influence of phase lag of heat flux $\bar{\tau}_q$ on transient axial thermal stress distribution in a hollow cylinder with $\bar{r}_{in} = 0.5$ when $\bar{t} = 0.06$.

Obviously, the phase lag of heat flux strongly affects the axial thermal stress distribution. Moreover, the thermal stress is sensitive to fractional order α. Fractional heat conduction with $0 < \alpha < 1$ does not show a serious jump of thermal stress, which can be clearly seen for a hyperbolic heat conduction model ($\alpha = 1$). The latter arises from the effect of reflected heat waves from the outer surface.

When analyzing crack problems, the SIF is a very important fracture parameter to describe the intensity of elastic stress fields near the crack front. By solving Eqs. (66) and (67), the transient SIFs for an embedded internal circumferential crack in a hollow cylinder with normalized inner radius $\bar{r}_{in} = 0.5$ can be obtained

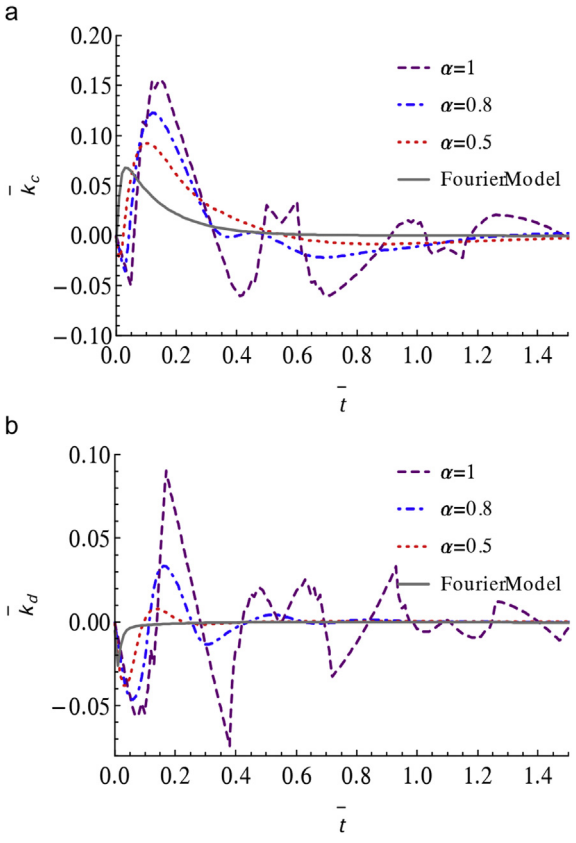

Fig. 8. Effects of fractional order α on thermal SIF history for (a) crack front at $\bar{r} = \bar{c}$ (b) crack front at $\bar{r} = \bar{d}$ for an embedded circumferential crack in a hollow cylinder with $\bar{r}_{in} = 0.5$, $\bar{c} = 0.6$ and $\bar{d} = 0.8$.$\bar{\tau}_q = 0.3$.

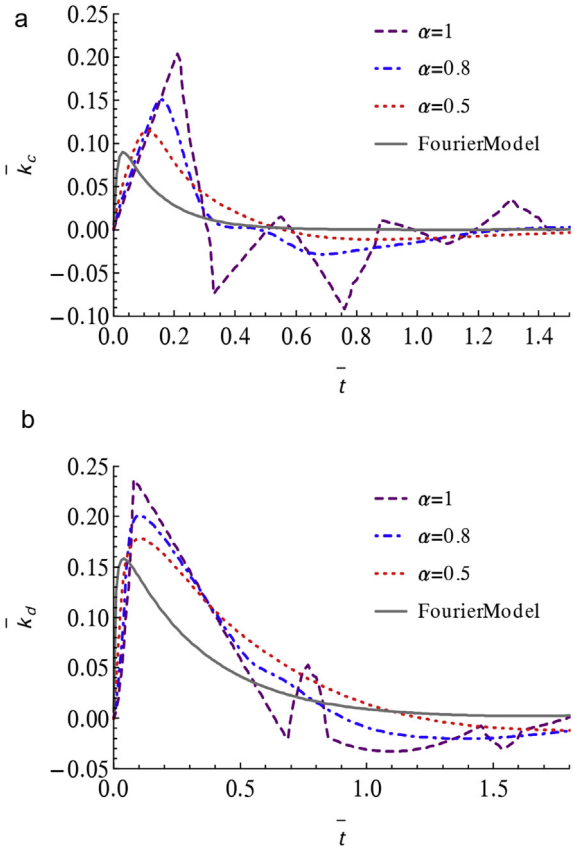

Fig. 9. Transient thermal SIF history near the crack front for (a) a circumferential outer surface crack in a hollow cylinder with $\bar{r}_{in} = 0.5$ and (b) a circumferential inner surface crack in a hollow cylinder with $\bar{r}_{in} = 0.3$ when $l_c/h = 0.2$ and $\bar{\tau}_q = 0.3$.

Table 1
Maximum SIF $\overline{K}_I^c$ for an outer surface circumferential crack in a hollow cylinder with $\bar{r}_{in} = 0.5$ when heated at the inner surface.

τ_q	α	l_c/h						
		0.01	0.1	0.2	0.3	0.4	0.5	0.6
0		0.0188	0.0617	0.0900	0.1123	0.1303	0.1448	0.1585
0.3	1.0	0.0528	0.1531	0.2040	0.2480	0.2677	0.2768	0.2930
	0.8	0.0346	0.1096	0.1509	0.1790	0.1988	0.2127	0.2220
	0.5	0.0247	0.0804	0.1151	0.1401	0.1590	0.1736	0.1847
0.8	1.0	0.0556	0.1685	0.2224	0.2601	0.2790	0.3016	0.3005
	0.8	0.0365	0.1152	0.1582	0.1864	0.2059	0.2193	0.2277
	0.5	0.0254	0.0826	0.1181	0.1434	0.1621	0.1764	0.1873

numerically. Under cold thermal shock ($T_a < T_0$) on the inner surface, the variation of the non-dimensional thermal SIFs near two crack fronts with normalized time is shown in Fig. 8a,b for an internal circumferential crack with $\bar{c} = 0.6$ and $\bar{d} = 0.8$. By comparing Fig. 8a with 8b, we find a noticeable difference, if adopting the classical Fourier model, two crack fronts have opposite trend, i.e. a positive thermal SIF near the inner crack front $r = c$ implies that it has a destructive effect on crack growth, whereas a negative thermal SIF near the outer crack front $r = d$ implies that it plays a shielding role. Nonetheless, for non-Fourier fractional order heat conduction model, two crack fronts basically have a similar trend with somewhat discrepancy lying in the response time and intensity of thermal SIF because of difference of arrival of reflected heat waves.

Fig. 9a shows transient thermal SIF history near the crack front for an outer surface circumferential crack in a hollow cylinder, where the crack length and phase lag of heat flux are set to be $l_c/h = 0.2$ and $\bar{\tau}_q = 0.3$. Here $h = 1 - \bar{r}_{in}$ is denoted as the non-dimensional wall thickness of the cylinder and $l_c = \bar{d} - \bar{c}$ is the normalized crack length. The hollow cylinder is still assumed to have non-dimensional inner radius $\bar{r}_{in} = 0.5$ and is suddenly heated at the inner surface. With the fractional order α increasing, the magnitude of SIF becomes larger and the wave behaviors are more serious. Here we calculate the maximum SIF or the overshoot of thermal SIF for an outer surface circumferential crack with various geometries, and numerical results are tabulated in Table 1. Obviously, the overshoot of thermal SIF is related to the fractional order α and phase lag of heat flux $\bar{\tau}_q$. Moreover, the overshoot of thermal SIF increases with fractional order α, phase lag of heat flux and the crack length. In an analogous manner, transient thermal SIF history near the crack front for an inner surface circumferential crack is depicted in Fig. 9b when a cracked cylinder with non-dimensional inner radius $\bar{r}_{in} = 0.3$ is cooled at the inner surface. The overshoot of thermal SIF is also calculated and listed in Table 2. Different from the results of an outer surface circumferential crack, the overshoot of thermal SIF near the inner surface crack front at first increases and then decreases with l_c/h rising. In Table 2 we also give the corresponding results obtained in Ref. [17] in parenthesis, which have been re-normalized to meet the same requirement. By comparison, we find that our results agree well with those [17].

6. Conclusions

Using a new generalized fractional heat conduction theory, we studied a transient thermal stress problem for a hollow cylinder with a circumferential crack. The analytical expressions for the temperature and thermal stress for an uncracked hollow cylinder

Table 2
Maximum SIF $\overline{K}_I^d$ for an inner surface circumferential crack in a hollow cylinder with $\bar{r}_{in} = 0.3$ when cooled at the inner surface.

τ_q	α	l_c/h						
		0.01	0.1	0.2	0.3	0.4	0.5	0.6
0		0.0802	0.1664	0.1582	0.1327	0.1037	0.0750	0.0480
		(0.0808)	(0.1642)	(0.1544)	(0.1272)	(0.0966)	(0.0662)	(0.0372)
0.3	1.0	0.0895	0.2198	0.2370	0.2320	0.2118	0.1861	0.1659
		(0.0898)	(0.2162)	(0.2352)	(0.2252)	(0.2042)	(0.1772)	(0.1534)
	0.8	0.0879	0.1951	0.2010	0.1835	0.1579	0.1290	0.0983
	0.5	0.0849	0.1801	0.1780	0.1559	0.1278	0.0980	0.0682
0.8	1.0	0.0905	0.2213	0.2487	0.2437	0.2312	0.2064	0.1791
	0.8	0.0877	0.1977	0.2062	0.1907	0.1665	0.1381	0.1075
	0.5	0.0853	0.1815	0.1805	0.1590	0.1312	0.1015	0.0713

Note: results in parenthesis are taken from Ref. [17].

were derived in the Laplace domain when the inner surface is subjected to a thermal shock and the outer surface is insulated. The transient temperature and thermal stresses in time domain were numerically calculated by numerical inversion of the Laplace transform. The thermal SIFs for an embedded circumferential crack, an inner surface crack and an outer surface crack were obtained, respectively. The effects of fractional order, normalized phase lag of heat flux and crack geometry on transient temperature change, thermal stresses and SIFs were analyzed, and the results are illustrated graphically. In particular, all these results were compared with those based on the classical Fourier heat conduction model and the hyperbolic heat conduction model, which can be taken as two special cases of the present model. The following conclusions can be drawn:

(a) With the increasing of fractional order α, temperature and thermal stresses exhibit wave-like behaviors. Specially for $\alpha = 1$ (the hyperbolic model), the response curves have sharp jumps at certain positions which correspond to the time period during which waves travel from the reflected surfaces. And at a certain location, the thermal stresses are compressive or tensile in an alternative way for the generalized fractional heat conduction model.
(b) With a larger phase lag of heat flux $\overline{\tau}_q$ for same fractional order, the jumps of curves of temperature change and thermal stress are more serious.
(c) Due to the wave-like behaviors, thermal SIFs have a striking difference with the classical Fourier heat conduction model for the inner surface being heated or cooled. With the fractional order α increasing, the magnitude of SIF becomes larger and the wave behaviors are more serious. The generalized fractional heat conduction theory is very necessary for analyzing crack problems in a hollow cylinder subject to hot and cold thermal shocks.

Acknowledgements

This work was supported by the National Natural Science Foundation of China (Nos. 11672336 and U1534207).

Appendix A

The functions Δ_j $(i,j = 1,2,3,4)$ and Δ used in Eq. (52) are given as follows:

$$\Delta_1 = \begin{vmatrix} Y_1 & b_{12} & b_{13} & b_{14} \\ Y_2 & b_{22} & b_{23} & b_{24} \\ Y_3 & b_{32} & b_{33} & b_{34} \\ Y_4 & b_{42} & b_{43} & b_{44} \end{vmatrix}, \quad \Delta_2 = \begin{vmatrix} b_{11} & Y_1 & b_{13} & b_{14} \\ b_{21} & Y_2 & b_{23} & b_{24} \\ b_{31} & Y_3 & b_{33} & b_{34} \\ b_{41} & Y_4 & b_{43} & b_{44} \end{vmatrix},$$

$$\Delta_3 = \begin{vmatrix} b_{11} & b_{12} & Y_1 & b_{14} \\ b_{21} & b_{22} & Y_2 & b_{24} \\ b_{31} & b_{32} & Y_3 & b_{34} \\ b_{41} & b_{42} & Y_4 & b_{44} \end{vmatrix}, \quad \Delta_4 = \begin{vmatrix} b_{11} & b_{12} & b_{13} & Y_1 \\ b_{21} & b_{22} & b_{23} & Y_2 \\ b_{31} & b_{32} & b_{33} & Y_3 \\ b_{41} & b_{42} & b_{43} & Y_4 \end{vmatrix},$$

$$\Delta = \begin{vmatrix} b_{11} & b_{12} & b_{13} & b_{14} \\ b_{21} & b_{22} & b_{23} & b_{24} \\ b_{31} & b_{32} & b_{33} & b_{34} \\ b_{41} & b_{42} & b_{43} & b_{44} \end{vmatrix},$$

where

$$b_{11} = \xi^2[-\xi I_0(\xi) + I_1(\xi)]$$

$$b_{12} = \xi^2[-\xi K_0(\xi) - K_1(\xi)]$$

$$b_{13} = \xi^2[(2\nu-1)I_0(\xi) - \xi I_1(\xi)]$$

$$b_{14} = \xi^2[-(2\nu-1)K_0(\xi) - \xi K_1(\xi)]$$

$$b_{21} = \xi^3 I_1(\xi)$$

$$b_{22} = -\xi^3 K_1(\xi)$$

$$b_{23} = \xi^2[\xi I_0(\xi) - 2(\nu-1)I_1(\xi)]$$

$$b_{24} = \xi^2[-\xi K_0(\xi) - 2(\nu-1)K_1(\xi)]$$

$$b_{31} = \xi^2\left[-\xi I_0(\xi\overline{r}_{in}) + \frac{1}{\overline{r}_{in}} I_1(\xi\overline{r}_{in})\right]$$

$$b_{32} = \xi^2\left[-\xi K_0(\xi\overline{r}_{in}) - \frac{1}{\overline{r}_{in}} K_1(\xi\overline{r}_{in})\right]$$

$$b_{33} = \xi^2[(2\nu-1)I_0(\xi\overline{r}_{in}) - \xi\overline{r}_{in} I_1(\xi\overline{r}_{in})]$$

$$b_{34} = \xi^2[-(2\nu-1)K_0(\xi\overline{r}_{in}) - \xi\overline{r}_{in} K_1(\xi\overline{r}_{in})]$$

$$b_{41} = \xi^3 I_1(\xi\overline{r}_{in})$$

$$b_{42} = -\xi^3 K_1(\xi\overline{r}_{in})$$

$$b_{43} = \xi^2[\xi\overline{r}_{in} I_0(\xi\overline{r}_{in}) - 2(\nu-1)I_1(\xi\overline{r}_{in})]$$

$$b_{44} = \xi^2[-\xi\overline{r}_{in} K_0(\xi\overline{r}_{in}) - 2(\nu-1)K_1(\xi\overline{r}_{in})]$$

$$Y_1 = 2(1-\nu)I_1(\xi\overline{r}_0)K_1(\xi) - \overline{r}_0\xi I_0(\xi\overline{r}_0)K_1(\xi) + \xi I_1(\xi\overline{r}_0)K_0(\xi) + \xi^2 I_1(\xi\overline{r}_0)K_1(\xi) - \overline{r}_0\xi^2 I_0(\xi\overline{r}_0)K_0(\xi)$$

$$Y_2 = \xi^2[I_1(\xi\overline{r}_0)K_0(\xi) - \overline{r}_0 I_0(\xi\overline{r}_0)K_1(\xi)]$$

$$Y_3 = \frac{2(1-\nu)}{\overline{r}_{in}} I_1(\xi\overline{r}_{in})K_1(\overline{r}_0\xi) - \xi I_0(\xi\overline{r}_{in})K_1(\overline{r}_0\xi) + \frac{1}{\overline{r}_{in}}\xi\overline{r}_0 I_1(\xi\overline{r}_{in})K_0(\overline{r}_0\xi) + \overline{r}_{in}\xi^2 I_1(\xi\overline{r}_{in})K_1(\overline{r}_0\xi) - \overline{r}_0\xi^2 I_0(\xi\overline{r}_{in})K_0(\overline{r}_0\xi)$$

$$Y_4 = \xi^2[-\overline{r}_{in} I_0(\xi\overline{r}_{in})K_1(\overline{r}_0\xi) + \overline{r}_0 I_1(\xi\overline{r}_{in})K_0(\overline{r}_0\xi)].$$

References

[1] Nied HF, Erdogan F. Transient thermal stress problem for a circumferentially cracked hollow cylinder. J Therm Stress 1983;6(1):1–14.
[2] Nied HF. Thermal shock in a circumferentially cracked hollow cylinder with cladding. Eng Fract Mech 1984;20(1):113–37.
[3] Meshii T, Watanabe K. Maximum stress intensity factor for a circumferential crack in a finite-length thin-walled cylinder under transient radial temperature distribution. Eng Fract Mech 1999;63(1):23–38.
[4] Meshii T, Watanabe K. Stress intensity factor of a circumferential crack in a thick-walled cylinder under thermal striping. J Press Vessel Technol 2004;126(2):157–62.
[5] Kordisch H, Talja H, Neubrech G. Analysis of initiation and growth of a circumferential crack in the HDR-RPV-cylinder under pressurized thermal

shock. Nucl Eng Des 1990;124(1):171–92.
[6] Dag S, Kadioglu S, Yahsi OS. Circumferential crack problem for an FGM cylinder under thermal stresses. J Therm Stress 1999;22(7):659–87.
[7] Nabavi SM, Ghajar R. Analysis of thermal stress intensity factors for cracked cylinders using weight function method. Int J Eng Sci 2010;48(12):1811–23.
[8] Eshraghi I, Soltani N. Thermal stress intensity factor expressions for functionally graded cylinders with internal circumferential cracks using the weight function method. Theor Appl Fract Mech 2015;80:170–81.
[9] Li X-F, Lee KY. Effect of heat conduction of penny-shaped crack interior on thermal stress intensity factors. Int J Heat Mass Transf 2015;91:127–34.
[10] Joseph DD, Preziosi L. Heat waves. Rev Mod Phys 1989;61(1):41.
[11] Lord HW, Shulman Y. A generalized dynamical theory of thermoelasticity. J Mech Phys Solids 1967;15(5):299–309.
[12] Mitra K, Kumar S, Vedavarz A, Moallemi MK. Experimental evidence of hyperbolic heat conduction in processed meat. J Heat Transf 1995;117(3):568–73.
[13] Tzou DY. A unified field approach for heat conduction from macro- to microscales. J Heat Transf 1995;117(1):8–16.
[14] Povstenko YZ. Fractional heat conduction equation and associated thermal stress. J Therm Stress 2004;28(1):83–102.
[15] Wang BL. Thermal shock resistance of solids associated with hyperbolic heat conduction theory. Proc R Soc A 2013;469(2153):926–30.
[16] Chen ZT, Hu KQ. Thermoelastic analysis of a cracked substrate bonded to a coating using the hyperbolic heat conduction theory. J Therm Stress 2014;37(3):270–91.
[17] Fu J, Chen Z, Qian L, Xu Y. Non-Fourier thermoelastic behavior of a hollow cylinder with an embedded or edge circumferential crack. Eng Fract Mech 2014;128:103–20.
[18] Fu J, Chen Z, Qian L, Xu Y. Thermal fracture of cracked cylinders associated with nonclassical heat conduction: the effect of material property. J Therm Stress 2016;39(9):1119–37.
[19] Korner C, Bergmann HW. The physical defects of the hyperbolic heat conduction equation. Appl Phys A 1998;67(4):397–401.
[20] Podlubny I. Fractional differential equations: an introduction to fractional derivatives, fractional differential equations, to methods of their solution and some of their applications, vol. 198. Academic press; 1998.
[21] Ortigueira MD. Fractional calculus for scientists and engineers, vol. 84. Springer Science & Business Media; 2011.
[22] Sherief HH, El-Sayed AMA, Abd El-Latief AM. Fractional order theory of thermoelasticity. Int J Solids Struct 2010;47:269–75.
[23] Youssef HM. Theory of fractional order generalized thermoelasticity. J Heat Transf 2010;132(6):061301.
[24] Povstenko Y. Fractional Cattaneo-type equations and generalized thermoelasticity. J Therm Stress 2011;34(2):97–114.
[25] Compte A, Metzler R. The generalized Cattaneo equation for the description of anomalous transport processes. J Phys A Math Gen 1997;30(21):7277–89.
[26] Qi H, Liu J. Time-fractional radial diffusion in hollow geometries. Meccanica 2010;45(4):577–83.
[27] Ezzat M, El-Bary A. Effects of variable thermal conductivity and fractional order of heat transfer on a perfect conducting infinitely long hollow cylinder. Int J Therm Sci 2016;108:62–9.
[28] Povstenko Y. Fractional thermoelasticity. Springer; 2015.
[29] Zhang X-Y, Li X-F. Thermal shock fracture of a cracked thermoelastic plate based on time–fractional heat conduction. Eng Fract Mech 2017;171:22–34.
[30] Jumarie G. Derivation and solutions of some fractional Black-Scholes equations in coarse-grained space and time. Application to Merton's optimal portfolio. Comput Math Appl 2010;59(3):1142–64.
[31] Ezzat MA. Magneto-thermoelasticity with thermoelectric properties and fractional derivative heat transfer. Phys B 2011;406(1):30–5.
[32] Ezzat MA. Thermoelectric MHD with modified Fourier's law. Int J Therm Sci 2011;50(4):449–55.
[33] Erdogan F, Gupta GD, Cook T. Numerical solution of singular integral equations, Springer. 1973.
[34] Theocaris P, Ioakimidis N. Numerical integration methods for the solution of singular integral equations. Q Appl Math 1977;35:173–83.
[35] Krenk S. On the use of the interpolation polynomial for solutions of singular integral equations. Q Appl Math 1975;32:479–84.
[36] Durbin F. Numerical inversion of Laplace transforms: an efficient improvement to Dubner and Abate's method. Comput J 1974;17(4):371–6.